Vegard relation and Raman band reference data generated from bulk crystals of kesterite phase composition series $Cu_2ZnSnS_{4x}Se_{4-4x}$ (CZTSSe $0 \leq x \leq 1$)

Authors
Theodore D. C. Hobson[1‡*], Oliver S. Hutter[1,4‡], Nicole Fleck[1], Luke M. Daniels[2], Jonathan D. Major[1], Tat Ming Ng[3] and Ken Durose[1]

1. Stephenson Institute for Renewable Energy / Dept. Physics, University of Liverpool, Peach St, Liverpool, L69 7ZF, UK.
2. Department of Chemistry, University of Liverpool, Crown Street, Liverpool, L69 7ZD, UK.
3. Department of Chemistry/Centre for Sustainable Chemical Technologies, University of Bath, Bath BA2 7AY, UK. Now at: Department of Mathematics, Physics and Electrical Engineering,
4. Northumbria University at Newcastle, Ellison Place, Newcastle Upon Tyne, NE1 8ST, UK.
*Corresponding author.

Author Contributions
The manuscript was written with contributions from all authors. All authors have given approval to the final version of the manuscript. ‡These authors contributed equally.

Orcid IDs
Theodore D. C. Hobson https://orcid.org/0000-0002-0013-360X
Oliver S. Hutter https://orcid.org/0000-0002-8838-8956
Nicole Fleck https://orcid.org/0000-0001-7800-056X
Luke M. Daniels https://orcid.org/0000-0002-7077-6125
Jonathan D. Major https://orcid.org/0000-0002-5554-1985
Tat Ming Ng https://orcid.org/0000-0002-7634-2635
Ken Durose https://orcid.org/0000-0003-1183-3211

ABSTRACT
Solid solutions in the series $Cu_2ZnSnS_{4x}Se_{4-4x}$ (CZTSSe) are of interest for PV applications. The purpose of this work was to grow bulk crystalline samples over the whole composition range to allow the Vegard relation (lattice parameter variation with composition) and the systematic behaviour of Raman bands to be defined so as to generate reference data. Samples with $0 \leq x \leq 1$ were synthesised from the elements and grown into crystalline form from solution in either KCl/NaCl eutectic or elemental Sn. Details of the crystal growth outcomes, including the use of a quartz seed plate to make thick film samples, are described. Ordered kesterite type material was formed upon crystallisation and x-ray diffraction demonstrated linear Vegard relationships, with the lattice parameters varying with composition as, a (Å) = -0.268(3)x + 5.6949(17) and c (Å) = -0.516(6)x + 11.345(3). Raman spectroscopy yielded two dominant peaks, these being kesterite A modes associated with the Se and S modes in CZTSe and CZTS. These varied in wavenumber linearly as ω_{CZTSe} (cm^{-1}) = (44.6 ± 1.6)x + (194.6 ± 0.8) and ω_{CZTS} (cm^{-1}) = (7.1 ± 1.3)x + (329.0 ± 0.8). Crystallisation was also shown to promote ordering.

The variation of lattice parameters with composition exhibited significant differences to those in previous studies. Also while the S Raman modes behaviour differed from previous reports, the Se modes were similar. These differences are discussed.

INTRODUCTION

The kesterite family of semiconductors is the subject of intense research into making thin film photovoltaics. Both Cu_2ZnSnS_4 (CZTS)[1] and $Cu_2ZnSnSe_4$ (CZTSe)[2] have been used to make photovoltaic devices, but those having the highest efficiency are made from the solid solution of the two - namely $Cu_2ZnSnS_{4x}Se_{4-4x}$ (CZTSSe), where x is the fraction of S. Presently the performance record (12.6%) is held by thin film devices grown using CZTSSe having $x = 0.2$[3].

Thin films of CZTSSe are formed using a variety of methods, but for all of them there is generally some uncertainty as to whether the target composition has been achieved. For example, one method is to first form multilayers of the metals copper, zinc and tin, and then to chalcogenize them by heating in the presence of either sulfur or selenium vapour. Volatile compounds have the opportunity to escape during this process, and this can cause compositional change. Some processes use sulfurization followed by selenization, and the resulting composition depends on the extent of ion exchange. As a result, post-growth analysis of some kind is often used in order to verify the actual composition of the material formed.

These CZTSSe kesterites are unusual in that the x-ray diffraction (XRD) lattice parameters are not unique and are shared by the related binary compounds. In the case of CZTS, the (100) interplanar spacings are shared by both CZTS and ZnS. Moreover, the x-ray atomic scattering factors of Cu and Zn are very similar – and hence *both* discrimination between CZTS and its secondary phases, and the identification of ordering phenomena in CZTS are difficult, if not impossible by XRD alone[4]. For that reason, XRD studies of CZTSSe are usually combined with Raman studies that are more sensitive to secondary phases and ordering: The level of order in the material, i.e. whether the kesterite or disordered kesterite phase dominates, may be identified from the Raman signature. Additionally, if disorder is present then the full width at half maximum (FWHM) of the Raman bands is increased, allowing the level of disorder to be assessed further[5,6].

It is the purpose of this paper to generate high quality reference data for both XRD and Raman spectroscopy for a set of samples spanning the whole composition range $Cu_2ZnSnS_{4x}Se_{4-4x}$ ($0 \leq x \leq 1$ with intervals of 0.1). To generate the reference data and to avoid the compositional ambiguities of thin films we used bulk CZTSSe both in the form of as-synthesised feedstock material, and in the form of crystallised samples grown from solution in molten salt KCl/NaCl mixtures. The elemental composition of the crystallised samples was accurately determined with both energy-dispersive x-ray spectroscopy (EDX) and inductively-coupled plasma optical emission spectroscopy (ICP-OES). The resulting Vegard coefficients and composition dependence of the Raman signature will be of widespread fundamental use as a reference data set: it will allow simple measurements from thin films to be back-correlated to the exact composition with high accuracy.

Previous combined XRD and Raman studies of CZTSSe are limited. Nagaoka *et al.*[7] reported the lattice parameters and Raman spectra for stoichiometric polycrystalline CZTSSe solid solutions with x = 0, 0.2, 0,5, 0.8 and 1, identifying a linear Vegard relationship of a (Å) = -0.26x + 5.71 and c (Å) = -0.53x + 11.45. In a follow-on paper, the same group[8] reported XRD and Raman data for stoichiometric CZTSSe single crystals having sulfur fractions: x = 0, 0.2, 0.5, 0.8 and 1, but only reported the lattice parameters for the end members (x = 0 and x = 1). The Raman peak positions were not plotted as a function of composition in either paper so a quantitative trend was not reported. Grossberg *et al.*[9] reported Raman spectra for x = 0, 0.26, 0.55 and 0.75, identifying linear

trends in the evolution of Raman spectra, but did not carry out XRD on the same samples. He *et al.*[10] carried out XRD and Raman on a series of CZTSSe solid solutions produced from metal sulfide/selenide precursors by solid-state sintering, producing a Vegard relationship a (Å) = -0.28x + 5.68 and c (Å) = -0.55x + 11.38. He's Raman data behaved linearly in x: Adachi *et al.*[11] reviewed the physical data on of CZTSSe and compared the Raman data of both Grossberg *et al.*[9] and He *et al.*[10]: the combined data set gave expressions for the trends in Raman modes of ω_{CZTSe} (cm^{-1}) = 46.8x + 194.9 and ω_{CZTS} (cm^{-1}) = 12.2x + 324.5. The form of the data was described very well by a two-mode phonon model[11].

Overall, there is a need for a single full, combined XRD and Raman study spanning the full composition range $Cu_2ZnSnS_{4x}Se_{4-4x}$ (0 ≤ x ≤ 1), having a higher density of data points – and therefore greater accuracy - than has been previously reported.

Given that CZTSSe solidifies in a peritectic reaction with ZnS, growth of CZTSSe crystals from the melt is challenging[8]. Here, we prepared stoichiometric CZTSSe large-grained crystalline solids from solution in molten salts. In earlier work using salts, Grossberg *et al.* produced large-grained CZTSSe solid solutions from molten KI salt for a characterisation series[9], and the formation of CZTS crystallites from the KCl/NaCl eutectic was reported as a synthetic route by Ionkin *et al.*[12]. Also, the method has been used by Mellikov *et al.* to make macroscopic 'monograin' crystallites of CZTS[13]. Here we report the use of crystallisation from molten NaCl/KCl to form bulk crystals for the entire composition range $Cu_2ZnSnS_{4x}Se_{4-4x}$ (0 ≤ x ≤ 1 in steps of 0.1). This paper also includes some work on crystal growth nucleation onto a separate flat silica seed plate.

Metallographic analysis, XRD and Raman characterisation were carried out on both the as-synthesised feedstock and the resulting crystallised samples. We obtained linear Vegard relations and linear two-mode Raman band evolution with composition, thus providing higher accuracy reference data than has been previously available. We also observed an increase in kesterite phase ordering upon crystallisation of the feedstock material from molten salt mixtures.

METHODS

Synthesis of feedstock and crystal growth protocols. Polycrystalline feedstock of CZTSSe over the whole composition range 0 ≤ x ≤ 1 in steps of Δx = 0.1 was synthesised from the elements (Alfa Aesar: Cu - 3N, Zn - 5N, Sn - 3N, S - 3N, Se - 5N purity) in stoichiometric proportions via one-step synthesis in sealed quartz capsules evacuated to 10^{-5} mbar and heated in a single-zone furnace.

During synthesis, the sealed tubes were heated to 800°C at 1.5°C/min, to promote sulfurization of the metals without the build-up of dangerous vapour pressures. The capsules were then soaked at 800°C for 24 hrs before cooling to 350°C at 0.5°C/min. The final cooling to room temperature was done in the furnace with the power off. 350°C is above the reported order/disorder transition for CZTS (260°C)[14] and CZTSe (200°C)[15] and so the formation of the partially-disordered kesterite phase was expected.

For the crystallisation processes, quartz tubes were loaded with CZTSSe and the solvent, and evacuated to 10^{-5} mbar. The solvent was either a NaCl/KCl mixture (0 ≤ x ≤ 1), or elemental tin (x = 1 only). When NaCl/KCl was used as a solvent, it was in the molar ratio 1 KCl: 1 NaCl, the eutectic composition, melting at 660°C (confirmed by differential scanning calorimetry (DSC), Figure S1). Capsules were charged with CZTSSe and NaCl/KCl in the molar ratio 1:8, 1:16 and 1:32. For these runs, the capsules were held static in a 2-zone furnace and the temperature profile was changed as a function of time to progress the crystal growth as follows: Firstly the furnace was ramped at 5°C/min to 785°C for CZTSe (x = 0) and to 875°C for CZTS (x = 1). Interpolated peak temperatures were used for intermediate compositions. Secondly, starting with both zones at the peak temperature, the temperature of one zone was reduced by 10°C in order to establish a temperature gradient of 1°C /

cm over the capsule. Thirdly, both zones were then cooled simultaneously lowering the whole temperature profile of the furnace at 0.4°C / hr over a 55°C window. This window was chosen as the solidification temperature of the CZTSSe feedstock in the NaCl/KCl mix was not known, but it was assumed to lie somewhere between the melting point of the pure material (established by DSC, see results) and a point 55°C below this. For some runs using NaCl/KCl as a solvent, a quartz seed plate (1 x 1 cm^2) was placed in the capsule so as to nucleate crystal growth.

In addition to the use of NaCl/KCl, for the growth of the pure sulfur compound (x = 1), Sn was used as the solvent and was included in the capsule in the ratio 70 mol% CZTS to 30 mol% Sn, as reported in ref.[16]. For these runs, the capsules were drawn through a vertical furnace at a rate of 0.6 mm/hr. The peak temperature in the furnace was 900°C and the temperature gradient was 13°C/cm.

Characterisation. Before characterisation, the crystallised solid solutions grown in the NaCl/KCl mix were soaked in deionised water for several hours to remove residual salt. For DSC and powder XRD, samples were finely ground with a pestle and mortar. For powder XRD, vacuum grease was spread in a 15 x 15mm square on a glass slide, and the ground powder was tapped across the square to form a uniform layer. For energy dispersive X-ray spectroscopy (EDX), single-grain XRD and Raman study, samples were embedded in epoxy, mechanically polished with 0.3 μm alumina and then chemically polished with 2vol% Br in MeOH. Samples were prepared for ICP-OES through dissolution of ~10 mg of solid material, stirred at room temperature in a mixture of 1 ml 37 wt% conc. HCl and 2ml 70 wt% conc. HNO$_3$, then diluted in DI water to 4 vol% acid conc. ICP-OES was carried out on solutions with an Agilent 5110 ICP-OES spectrometer, with emission intensity linearly calibrated against standards at 5 known levels of concentration for each emission wavelength, for all elements. Samples of DI water and diluted acid were also analysed to determine background levels of the relevant elements in the solutions. We also attempted Rutherford backscattering analysis for the composition determination, but this was not successful due to the known problem of detecting a light element (in this case S) in a matrix of heavier elements.

DSC was carried out using a TA Instruments SDT-Q600 with a heating rate of 5°C/min using alumina crucibles with lids. Samples were prepared for powder XRD by manual grinding with a pestle and mortar for a period of 1 min for the feedstock and 15 mins for the crystallised samples. XRD was carried out using a Rigaku Smartlab X-ray diffractometer with the 1.540560 Å Kα$_1$ and 1.544390 Å Kα$_2$ Cu lines used when measuring the powdered feedstock and single crystal grains, while the monochromated 1.540560 Å Kα$_1$ Cu line only was utilised when measuring the powdered crystallised series. A step-scan acquisition mode was utilised, with increments of 0.01°. 0.5 mm and 10 mm apertures were used for single grain and powder XRD respectively. Rietveld refinement was carried out with the 'Fullprof' software suite[17], with a step size of 0.01°. An 8-coefficient polynomial was used to fit the pattern background. The initial structural parameters for the crystal structure are shown in Table 1, based on the structure reported in[18].

Atom	Wyckoff Site	x Position	y Position	z Position	B_{Iso} (Å^2)	Occupancy
Cu/Zn	2a	0	0	0	0.1	0.125
Cu/Zn	2c	0	1/2	1/4	0.1	0.125
Cu/Zn	2d	0	1/2	3/4	0.1	0.125
Sn	2b	0	0	1/2	0.1	0.125
Se	8g	0.755	0.757	0.8718	0.1	$0.5 \cdot (1-x)$
S	8g	0.755	0.757	0.8718	0.1	$0.5 \cdot x$

Initial	a (Å) =	-0.262 + 5.6965
Lattice	c (Å) =	-0.0497x + 11.3394
Parameters:		

Table 1. Initial structural parameters for Rietveld refinement of powder XRD patterns for CZTSSe. The values of B_{Iso} were not refined independently. Overall occupancy was fixed at 1 with ratios assuming stoichiometric composition and lattice parameter values were interpolated based on the values reported in Choubrac for CZTSe[19] and Ritscher for CZTS[18]. For the case of occupancy and lattice parameters, the value x refers to the quantity S/(S+Se) rather than x-position.

For the refinement, the I-4 crystal space group was applied, assuming a kesterite structure and in line with the methodology of Ritscher and Nozakia[18, 20]. S and Se were treated as occupying the same co-ordinates in the unit cell for all of the solid solutions, and the occupancy of the 2a, 2c and 2d Wyckoff sites with either Cu or Zn was treated as equivalent, since for the case of disordered kesterite, Cu or Zn may each occupy this site at random. Cu and Zn also have very similar x-ray scattering factors and atomic radii, meaning that distinguishing between them within CZTSSe using conventional XRD is unfeasible. It is therefore reasonable to treat the occupancies as interchangeable. Further details of the refinement methodology are in the SI. SEM and EDX were carried out with a JEOL JSM-7001F FESEM at 15kV, and the 'XPP' matrix correction was used in calculating the elemental proportions from EDX spectra. Raman spectroscopy was carried out with a Renishaw in-Via Raman microscope at 532 nm excitation wavelength with a beam power of 1 mW, a spot size of 2 μm with a 50x long-working-distance objective and a 1800 lines/mm grating. The maximum power of 1 mW was used to avoid heat-induced degradation, in line with the methodology applied in Valakh *et al.*[28]. Spectra were calibrated using a c-Si reference. The peaks in the Raman spectra were fitted to Lorentzian profiles.

RESULTS AND DISCUSSION

Synthesis and Crystal Growth Outcomes.

a) Synthesis of polycrstalline CZTSSe 'feedstock' from the elements.
Synthesis of polycrystalline CZTSSe feedstock from the elements in sealed tubes was successful for all compositions in the range $0 \leq x \leq 1$, as confirmed by powder XRD and Raman in later subsections. The feedstock took the form of dense, powdery black ingots, and were homogeneous on visual inspection. SEM indicated that the ingots consisted of crystal grains around 1 μm in size (an example for x = 0.5 is shown in Figure S2). EDX area scans were carried out for several samples across the $0 \leq x \leq 1$ composition range on 2 - 12 sites per sample. The size of scan areas were around 20 x 20 μm^2. Results were averaged, with the error given by the standard deviation. These results, shown in the SI (Table S1) confirmed that the composition of the feedstock was generally consistent with the compositions expected from weighing.

In order to select temperatures for the crystal growth, the melting points of the feedstock for samples across the composition range were measured. There was a linear relationship between the weighed sulfur fraction x and melting point (Figure 1) with the fit being T_{melt}(°C) = 87.9x + 775.6. This allows the interpolation of the melting points of CZTSSe solid solutions of known composition, at a DSC heating rate of 5°C/min.
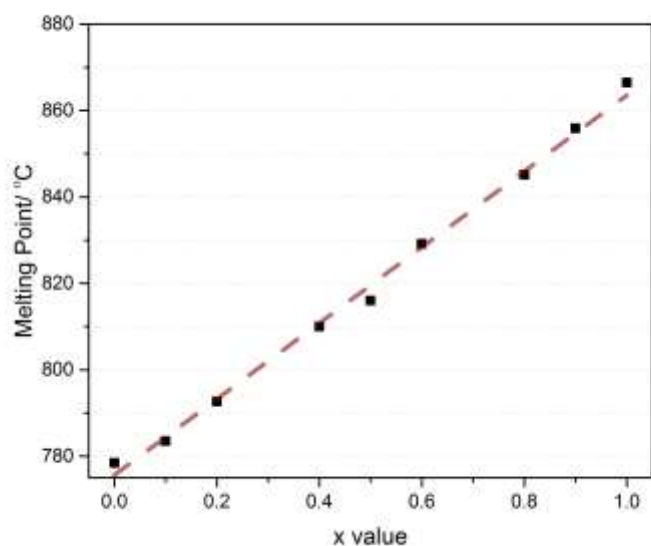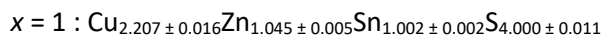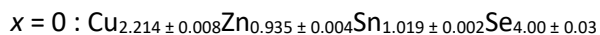
Figure 1. Melting points of $Cu_2ZnSnS_{4x}Se_{4-4x}$ feedstock as a function of weighed sulfur fraction x measured using differential scanning calorimetry at a heating rate of 5°C.

b) Growth of large-grained CZTSSe from KCl/NaCl molten salts.

Use of the feedstock above in formation of crystals of CZTSSe from the KCl/NaCl salt mix was successful across the whole composition range $0 \leq x \leq 1$, providing 10 crystal sets for analysis by EDX, XRD and Raman, all of which indicated formation of the compound.

Chemical analysis of the crystals was undertaken using EDX using the same protocols as for the feedstock, with 3 - 11 sites for each composition. However, the results (Table S2) show a greater degree of agreement between the measured and expected (target) compositions for the crystallised material than for the as-synthesised feedstock. The increased match in composition for the crystals is likely due to their being melt-grown, with the melting ensuring greater homogeneity in the material than was achieved through the solid-state synthesis process.

Furthermore, the measurements from ICP-OES are consistent with those of EDX (see Figures. S4 and S5), demonstrating the reliability of the former measurements while also indicating a overall agreement between the weighed ratios and the ratios present in the crystallised material. The main differences are that the ICP-OES indicates a greater Cu proportion than expected (~2 at%), leading to all samples being slightly metals-rich. Given that the matrix-correction step of EDX may give rise to systematic errors, the measured compositions from ICP-OES are used in subsequent quantitative analysis of the crystallised samples, even though there is close agreement between the two methods. For the crystallised end members, the elemental compositions were determined from ICP-OES as:

$x = 0$: $Cu_{2.214 \pm 0.008}Zn_{0.935 \pm 0.004}Sn_{1.019 \pm 0.002}Se_{4.00 \pm 0.03}$

$x = 1$: $Cu_{2.207 \pm 0.016}Zn_{1.045 \pm 0.005}Sn_{1.002 \pm 0.002}S_{4.000 \pm 0.011}$

The crystallised material comprised of compact deposits of CZTSSe on the walls of the growth tube around 0.5 mm thick, with a hard and smooth black surface and having compact crystal grains around 100 μm in size (a representative micrograph of $x = 0.3$ is shown in Figure S3a). The size of the crystal grains in these compact deposits did not vary significantly with x (a graph is shown in Figure S3b). In addition to nucleation on the walls, nucleation was observed within the melt, producing free CZTSSe monograins up to 700 μm in size (Figure S3c), distributed through the solvent volume upon cooling. Features resembling twin defects were observed in these monograins, indicated by straight

boundaries within the grains (see Figure S3c). Both the grains forming the compact deposit on the walls and the free grains nucleated in the solvent volume were significantly larger than the grains in the feedstock (Figure S2). XRD of polished monograin samples (Figure 3a,) produced single peaks indicating that they were indeed single crystal in nature. These large grains allow individual grains to be characterised using Raman microscope spectroscopy, with spot sizes on the order of μm. Raman spectroscopy has been carried out on single crystals of CZTSSe before, in the work of Nagaoka *et al.*[8]. Grossberg *et al.*[9] also succeeded in producing monograins larger than the laser spot size of a Raman system, allowing them to probe individual crystals. However, Nagaoka only reported lattice parameters for the end members, and Grossberg did not carry out XRD on their sample set. Therefore, to our knowledge, this work is the first to report single-crystal Raman combined with a report of lattice parameters across the same sample set.

c) Growth of thick film polycrystalline CZTSSe using quartz seed plates.

The growth of the compact deposits on the walls of the tube during crystallisation from KCl/NaCl indicated that nucleation could be encouraged by a quartz surface. As a result of this observation we placed a 1x1 cm^2 silica plate in the growth tube for some crystallisation runs in order to act as a seed plate. This resulted in thick-film deposits of CZTSSe about 0.5 mm thick and having the same black, smooth appearance as the deposits formed on the walls, but they were flat and 1 x 1 cm^2 in size making them more practical to handle. Polishing revealed crystal grains of around 100 μm in size, the same scale as for the compact deposits on the walls (see Figure S3d). This method could be developed further for the crystallisation of CZTSSe if crystals with a more useable shape are required than are formed on the walls of curved growth tubes.

d) Growth of CZTS from Sn.

The Sn-solvent growth of CZTS (x = 1) in the vertical furnace resulted in a multi-grained crystal 15 mm long. It contained 10 mm long columnar grains, oriented along the growth axis and 2 mm wide (see Figure 2b). XRD of individual grains produced single peaks confirming that the grains visible on the polished boules were indeed crystalline (see Figure 2a).

Both the feedstock and the crystallised solid solutions were judged suitable for further characterisation by XRD and Raman as reported below.
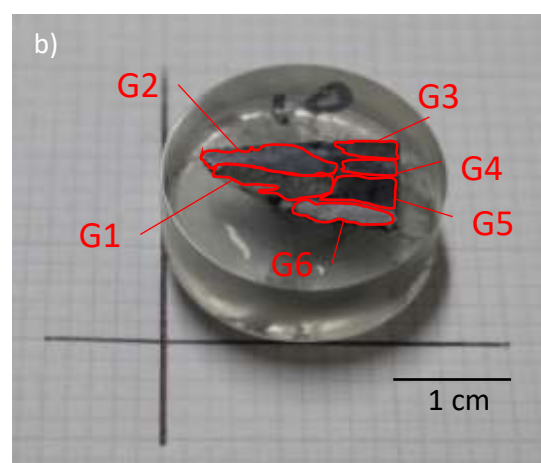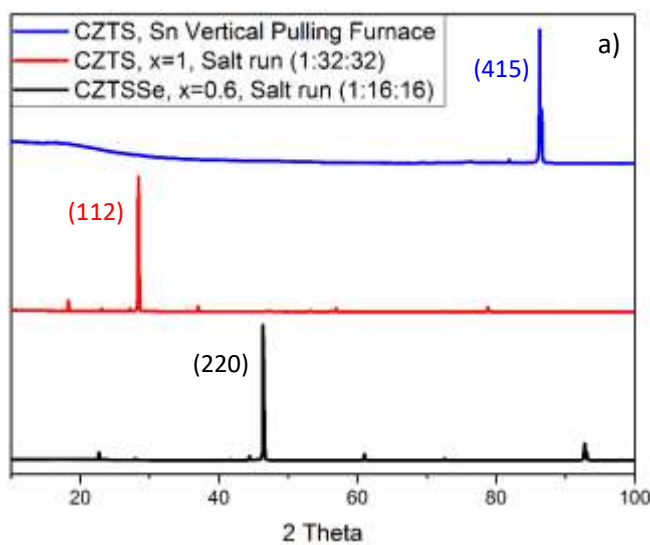
Figure 2. (a) XRD patterns for (bottom) crystallised $Cu_2ZnSnS_{4x}Se_{4-4x}$ solid solution (x = 0.6) grown in NaCl/KCl mix with ratio CZTSSe:NaCl:KCl of 1:16:16; (middle) crystalline CZTS (x = 1) grown in NaCl/KCl mix with ratio CZTSSe:NaCl:KCl of 1:32:32; (top) crystalline CZTS (x = 1) grown from Sn solution in vertical pulling furnace in ratio 70mol% CZTS to 30mol% Sn and (b) the sample for the latter showing the grain boundary positions.

XRD Investigation. The powder XRD $\theta - 2\theta$ scans for the CZTSSe feedstock are shown in Figures 3 a and b. These offer further evidence for the successful synthesis of CZTSSe through the presence of sharp, strong peaks consistent with the (112), (220) and (332) diffraction peaks for the series end members: at 27.14°, 45.05° and 53.33° for CZTSe (x = 0), and at 28.46°, 47.36° and 56.15° for CZTS (x = 1). As mentioned before, ZnS and ZnSe may also produce these peaks[4], but the Raman results discussed in the next subsection indicate very few secondary phases. Furthermore, the XRD scans indicate a smooth, linear shift in the position of the diffraction peaks with weighed sulfur content (x), suggesting a similar shift in the lattice parameters, and demonstrating the presence of a solid solution over the whole composition range.

The results for the crystallised CZTSSe solid solutions are similar to those from the feedstock, there being similar peak positions for the end members and a smooth shift of the peaks with x.

Conventional XRD is not directly sensitive to ordering in CZTSSe, although the work of Choubrac[22] suggests that small shifts in cell volume may result from relative order/disorder, due to changes in the c parameter.
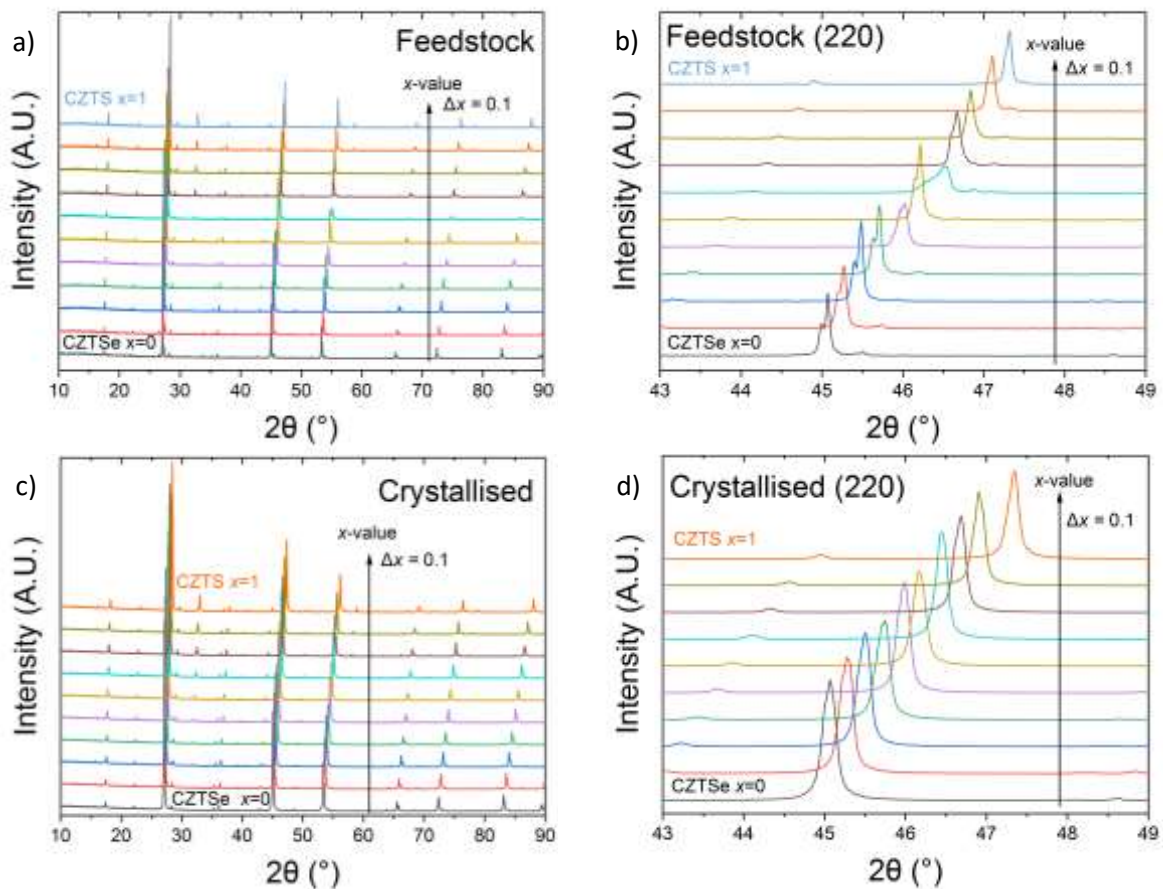
Figure 3. Powder XRD patterns: (a) $Cu_2ZnSnS_{4x}Se_{4-4x}$ feedstock where $0 \leq x \leq 1$ in increments of $x = 0.1$ based on weighed S-Se proportion. (112), (220) and (332) peaks are the 3 most prominent. There is a clear, linear shift in all major peaks towards higher angles with increased sulfur content, as made clear in the shift of the 220 peak (b). (c) Crystallised CZTSSe solid solutions grown in NaCl/KCl mix, where $0 \leq x \leq 1$ in 0.1 increments of x. (112), (220) and (332) peaks are the 3 most prominent. There is a clear linear shift in all major peaks towards higher angles with increased sulfur content, as exemplified by the shift of the 220 peak (d). The XRD was carried out with an un-monochromated $K\alpha_1$ and $K\alpha_2$ source for (a) and (b), yielding peaks as doublets, while a monochromated $K\alpha_1$ source was employed for (c) and (d), yielding singlet peaks.

Rietveld refinement was carried out on the powder XRD patterns for all compositions of both the feedstock and crystallised solid solutions in order to obtain the lattice parameters. To deal with samples over the composition range $0 < x < 1$, the initial lattice parameters and atomic positions for the refinements were interpolated from literature values for the two end members (see Methods, Table 1). This approach was assumed to be valid due to the observed linear shift in the position of the diffraction peaks with x. After refinement, the χ^2 values for the crystallised series patterns varied between 2 and 4 for the whole series, with the relevant fitting parameters fully listed in Table S2. Example refinement plots (with residuals) for the crystallised CZTSSe samples $x = 0$, 0.4, 0.6 and 1 are shown in Figure S6. The resulting refined values for lattice parameters, anion position and B_{Iso} are listed for all samples in the crystallised series in Table S3.

The lattice parameters for the end members CZTSe ($x = 0$) and CZTS ($x = 1$) obtained experimentally in this work are compared with literature values in Table 2. There is good agreement with the values in Adachi's review[11], those being the averages of published data. There is a small difference in unit cell volume between the two sample sets presented in this work, with the values for the CZTS ($x = 1$) feedstock larger than that for the crystallised. Based on Choubrac's work[22] this would suggest greater ordering in the crystallised CZTS samples compared to the feedstock, with the cell volumes for CZTS very similar to those reported by Choubrac (319.80 Å^3 for an ordered sample, 320.10 Å^3 disordered). In contrast, however, Choubrac *et al.* found the change in cell volume to result solely from changes in the c parameter, which is not the case in this work. The copper-rich nature of our samples (see previous section) compared to a composition closer to stoichiometry in Choubrac's work[22], may be a key factor in this different behaviour. The very similar values of cell volume between feedstock and crystallised CZTSe samples in this work offer no such indication of ordering behaviour. The effects of ordering may be characterised more directly via Raman, as in the following section, allowing us to explore this idea further.

It is known that the lattice parameters in CZTSSe are sensitive to cation ratios, with several CZTS compositions having been studied by Lafond[23]. Samples from that work which matched most closely with our samples for lattice parameters are shown in Table 2, along with a comparison of cation ratios.

Sample Set		Composition	
		CZTSe ($x = 0$)	**CZTS ($x = 1$)**
This work: feedstock	a / Å	5.69193(5)	5.43296(8)
	c / Å	11.34416(15)	10.84387(22)
	Cell volume / Å^3	367.529(7)	320.079(9)
This work: material crystallised in	a / Å	5.69258(3)	5.43170(3)
NaCl/KCl mix	c / Å	11.34351(8)	10.83919(8)
	Cell volume / Å^3	367.591(7)	319.792(6)
	Cu/(Zn+Sn)	1.13	1.07
	Zn/Sn	0.92	1.04

Adachi[11] – compiled data	*a* / Å	5.688	5.430
	c / Å	11.341	10.845
	Cell volume / Å³	366.92	319.76
Sample #3 – Lafond[23]	*a* / Å		5.43006
	c / Å		10.8222
	Cell volume / Å³		319.098
	Cu/(Zn+Sn)		0.79
	Zn/Sn		1.19
Sample #4 – Lafond[23]	*a* / Å		**5.43097**
	c / Å		10.8415
	Cell volume / Å³		**319.777**
	Cu/(Zn+Sn)		0.95
	Zn/Sn		1.08
Sample #6 – Lafond[23]	*a* / Å		5.42936
	c / Å		**10.8391**
	Cell volume / Å³		319.53
	Cu/(Zn+Sn)		1.14
	Zn/Sn		0.8

Table 2. Lattice parameters and cell volumes of the pure sulfide and selenide materials synthesised in this work, compared to the literature values reported in the review by Adachi[11], these being the average of the experimental values available, and in the study by Lafond on sensitivity of lattice parameters to cation composition[23]. Parameters in the latter study that match most closely to our results are in bold.
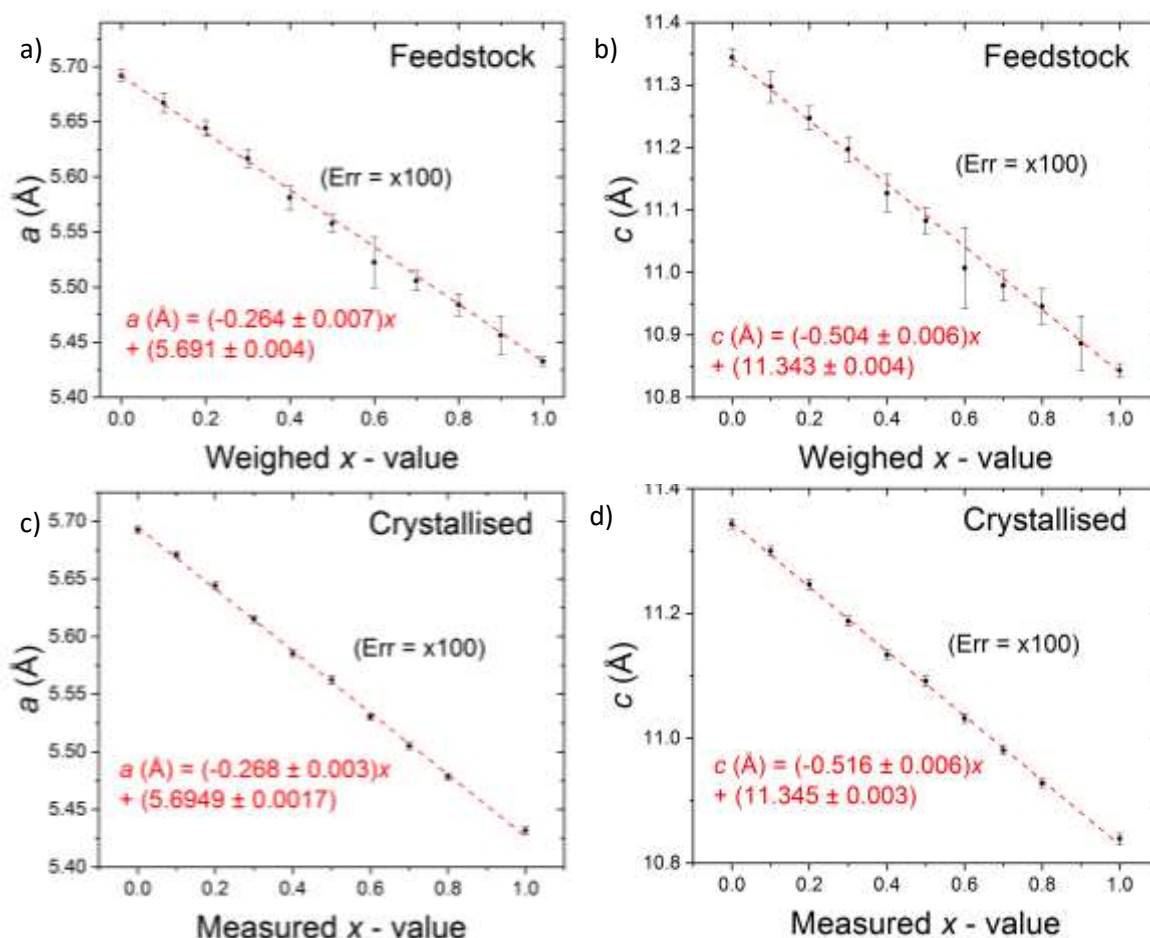
Figure 4. Lattice parameters a and c for $Cu_2ZnSnS_{4x}Se_{4-4x}$ ($0 \leq x \leq 1$). Data for the as-synthesised feedstock are shown in (a) and (b) respectively, (weighed x values) and for the crystallised materials in (c) and (d), with x values based on the elemental ratios measured with ICP-OES (see Table S1). The values were extracted from the XRD patterns by Rietveld refinement. Both sets of samples show linear Vegard relationships, indicating that solid-solutions are formed. The equations of the best linear fits are shown on the graphs. The error bars displayed on all plots are 100x larger than the real uncertainties on the lattice parameter values, in order to allow comparison of the uncertainty between data points.

The lattice parameter values at all x-compositions are plotted in Figure 4, for the feedstock a) and b) and crystallised solid solutions c) and d). These all obey linear Vegard relationships. The lines of best fit were, for the feedstock: a (Å) = -0.264(7)x + 5.691(4) and c (Å) = -0.504(6)x + 11.343(4), and for the crystallised materials: a (Å) = -0.268(3)x + 5.6949(17) and c (Å) = -0.516(6)x + 11.345(3). Nagaoka *et al.* reported the fit as a (Å) = -0.26x + 5.71 and c (Å) = -0.53x + 11.45[7], while He *et al.*[10] found a (Å) = -0.28x + 5.68 and c (Å) = -0.55x + 11.38. The lines for all four fits are shown together for comparison in Figure S7. For our work, the number of significant figures for the fits above is reported so as to be self-consistent with the goodness of the linear fits. (Since the fits were better for the a parameter data than for c the former are quoted with higher precision).

For the materials made in this study, the lattice parameter data from both the as-synthesised feedstock and the crystallised materials were in close agreement. The samples reported by Nagaoka *et al.* [7] had lattice parameters that were systematically higher than our values, the differences being approximately +0.02 Å in a and +0.1 Å in c across the whole composition range. However, the present data and the data of He *et al.*[10] differ for the behaviour of a and c: The values of a from He *et*

al. are always lower than our own but the difference increases from -0.01 to -0.03 Å as x increases from 0 to 1. On the contrary, the values of c are greater than our own, being +0.04 Å higher at x = 0, and converging with ours at x = 1. These trends are compared graphically in Figure S7.

These discrepancies between the Vegard relations have an impact on the values of composition that may be estimated from XRD measurements on thin films. Findings for the mid composition x = 0.5 illustrate the point: If c is used, then compared to our data, the data of Nagaoka *et al.*[7] overestimate x by 0.19, while He *et al.* yield comparable results. If a is used then the data of Nagaoka *et al.* overestimate x by 0.08 while He *et al.* underestimate it by 0.07.

Reasons for the systematic differences in lattice parameter from study to study (Figure S7) may lie in deviations from stoichiometry which are known to influence precision lattice parameters even in binary compounds. Kesterites are known to support quite large stoichiometric deviations, for example, the samples of Nagaoka *et al.* had 0.91 < Cu/(Zn+Sn) < 0.96, 1.69 < Cu/Zn < 1.76 and 1.13 < Zn/Sn < 1.26[7] while the samples in the present work had ratios closer to values of 1.1, 2.2 and 1 respectively (Table S1). However, without dedicated experiments the origin of the systematic error cannot be determined. Nevertheless we can state with certainty that the Vegard's relations established for our samples have higher self-consistent precision than earlier reports as a result of the higher number of data points obtained, our linear relations being defined and reported to three or four decimal places, whereas in earlier works results were plotted but not reported numerically, allowing values to be read-off to only 2 decimal places.

Raman Investigation. Raman spectra were taken for the end members CZTSe (x = 0) and CZTS (x = 1) from both the CZTSSe feedstock and material crystallised from the NaCl/KCl melt. The samples were set in resin blocks and polished to produce flat surfaces for characterisation.

a) Raman of the end members CZTSe and CZTS (x = 0 and 1)

The Raman spectra for feedstock and the crystallised solid solutions grown in NaCl/KCl are shown in Figure 5 for the end members CZTSe (x = 0) in a) and b) and CZTS (x = 1) c) and d) respectively.
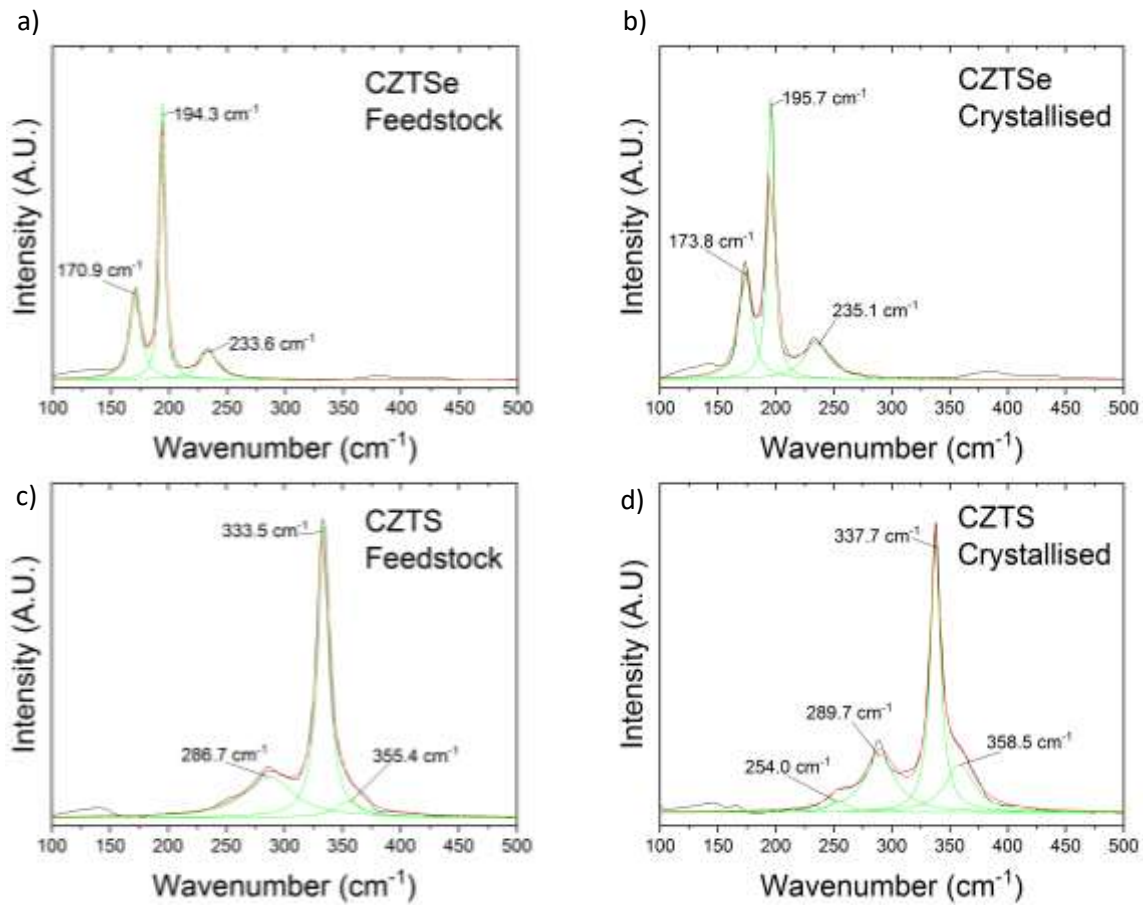
Figure 5. Raman spectra for CZTSe are shown in (a) (feedstock) and (b) (crystallized material). All peaks move to slightly higher wavenumbers in the recrystallized material and the peak at 171-174 cm^{-1} intensifies. Peaks for CZTS are shown in (c) (feedstock) and (d) (crystallized material). For the feedstock material (c) the principal peak at 333.5 cm^{-1} lies between the expected values for disordered kesterite at 331 cm^{-1} and ordered kesterite at 337cm^{-1} [5,15], with the peak at 355.4 cm^{-1} possibly due to Cu_2SnS_3[21] or ZnS[24]. For the crystallised CZTS (d) a principal peak at 337.7 cm^{-1} was present, suggesting more ordered kesterite, with a slight narrowing in the FWHM compared to the feedstock material (10.7 cm^{-1} compared to 11.8 cm^{-1}). The shoulder at 358.5 cm^{-1} suggests the presence of Cu_2SnS_3[21], or ZnS[24], or a combination, as phase impurities.

The spectrum for the CZTSe (x = 0) feedstock shows clear peaks at 170.9 and 194.3 cm^{-1} with a smaller peak at 233.6 cm^{-1}. All three peaks are consistent with literature reports for solution-processed CZTSe thin films, for example, one utilising electrodeposition[25] and another using spray pyrolysis[26] – which place a peak at around 235 cm^{-1}. Meanwhile, data compiled by Adachi[11], averaged across multiple studies, assigns the symmetry modes A_1, A_1 and B_1 to peaks at 170 cm^{-1}, 195 cm^{-1} and 231 cm^{-1} respectively, suggesting that these are the modes represented in our work at 170.9 cm^{-1} (A_1), 194.3 cm^{-1} (A_1) and 233.6 cm^{-1} (B_1). The 233.6 cm^{-1} peak may also comprise small peaks resulting from Cu_2SnS_3, at 236 and 251 cm^{-1}. The peak for pure selenium at 232 cm^{-1} (Rruff ID: R060137.2), could not be ruled out, although the laser irradiance of ~ 0.3 mW μm^{-2} was not expected to induce decomposition of the CZTSe. For the CZTSe crystallised in the NaCl/KCl mix, the Raman spectrum is similar to the feedstock, but shifted to a higher wavenumber for all peaks. Such an upward shift has also been reported by Rey[15], where a principal peak at 194.6 cm^{-1} was associated

with disordered kesterite, and a peak at 196.4 cm^{-1} with ordered kesterite. Additionally, the theoretical work of Khare *et al.*[27] predicts higher values for the A mode in kesterite CZTSe compared to the A$_1$ mode present in disordered kesterite. For this reason we assigned the kesterite symmetry modes A, A and B to the 173.8 cm^{-1}, 195.7 cm^{-1} and 235.1 cm^{-1} peaks respectively.

The Raman spectrum for the end member CZTS (*x* = 1) is shown for the feedstock in Figure 5c. The peak value at 286.7 cm^{-1} is consistent with reported experimental values for kesterite CZTS[24], Meanwhile the peak at 355.4 cm^{-1} may correspond to the ZnS[24] or Cu$_2$SnS$_3$[21] secondary phases. Elemental sulfur peaks at 154, 220, 436 and 473 cm^{-1} (Rruff ID: R040135.2) were, in general, not observed, although a small bump at ~250 cm^{-1} may correspond to the 247 cm^{-1} sulfur peak. Nonetheless, the spectrum is certainly not dominated by S peaks, confirming that the laser has not decomposed the sample, which is expected for the low irradiance. The strong peak at 333.5 cm^{-1} appears to be intermediate between the 331 cm^{-1} peak mentioned in the work of Valakh *et al.*[28] where it is associated with the disordered kesterite A$_1$ mode, and a peak position of 337 cm^{-1}, associated with the kesterite A mode [5]. This strongly suggests that the CZTS feedstock takes the form of partially disordered kesterite, with the distribution of Cu and Zn cations on the 2c and 2d Wyckoff positions intermediate between being fully ordered and fully random[5,6]. The idea of coexisting kesterite A mode and the A$_1$ mode of disordered kesterite, is consistent with the work of Grossberg *et al.* for CZTS (*x* = 1) and their interpretation[5].

In contrast, the principal peak is positioned at 337.7 cm^{-1} in the Raman spectrum for the CZTS crystallised in NaCl/KCl (Figure 5d). This shift to higher wavenumber, similar to the behaviour observed in the CZTSe, suggests that the crystallised CZTS material adopted a more ordered kesterite configuration. A greater level of order in the crystallised samples most likely comes as a result of the slow-cooling step (see methods), as in Choubrac[22], where the most ordered sample was cooled at the slowest rate. The peak at 358.5 cm^{-1} may also result from ZnS[24], Cu$_2$SnS$_3$[21], or a combination.

b) Raman of the full composition series 0 ≤ *x* ≤ 1

Raman spectra were taken for the whole composition series (0 ≤ *x* ≤ 1) of crystallised CZTSSe feedstock. The narrow FWHM for the peaks in the spectra for the crystallised material allowed the wavenumber of the vibrational modes to be fitted to high precision, with these results shown in Figure 6a and b.
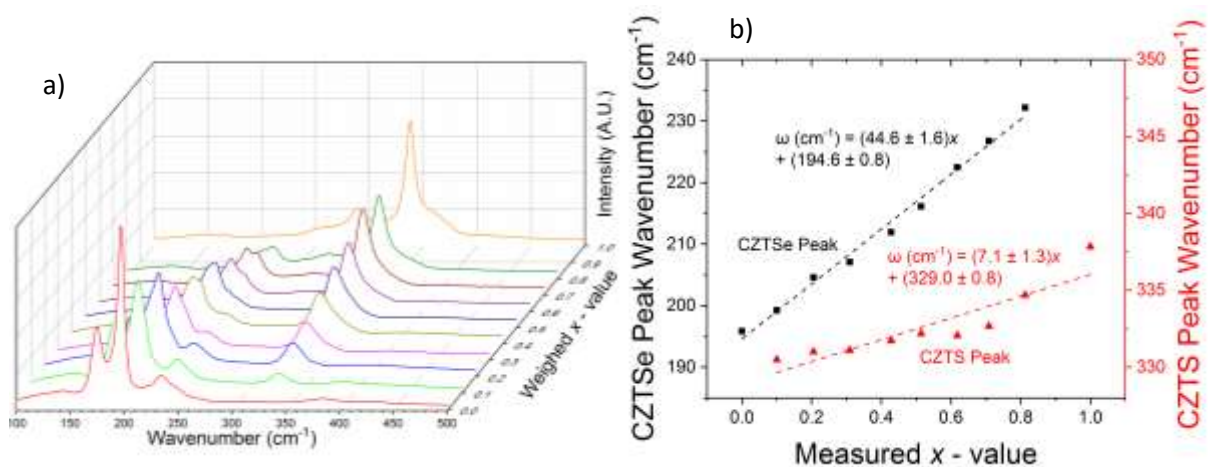

Figure 6. (a) Raman spectra for the Cu$_2$ZnSnS$_{4x}$Se$_{4-4x}$ solid solutions crystallised from KCl/NaCl (weighed *x* – value). (b) Position of principal peaks (A mode) for crystallised solid solutions, with *x* -

value measured via ICP-OES, illustrating the shift to higher wavenumber peak with changing compositions from selenide to sulfide.

These results show a clear evolution in the positions of the most intense peaks (assigned to the A kesterite modes) with composition. Also, the peaks for solid solutions of intermediate compositions have higher full-widths at half-maxima (FWHM) than those of the end members. Both the 'CZTSe-like' and 'CZTS-like' vibrational modes shift towards higher wavenumbers with increasing x-value, following a linear trend as shown in Figure 6b. The increased FWHM of the peaks at intermediate compositions relative to the end members (Figure S8) most likely results from anion disorder.

As expected, the solid solutions show 'two-mode' behaviour for which the spectra comprise modes dominated by *either* sulfur or selenium atoms, as discussed by Grossberg *et al.*[9] and Adachi[11]. The two-mode behaviour may be understood by applying the modified random-element isodisplacement model (outlined by Chang and Mitra[29]) and treating the CZTSe-CZTS system as a pseudobinary: AB_xC_{1-x} where A is Cu2SnZn with mass $M_{Cu2ZnSn} = M_{Cu2} + M_{Zn} + M_{Sn}$, while S_4 and Se_4 are treated as B and C respectively. The two-mode behaviour is expected for CZTSSe within this model since, as outlined by Adachi[11], the mass of sulfur is smaller than the reduced mass for the A-C ($M_{Cu2ZnSn}$ and M_{Se}) system, meaning the criterion for two-mode behaviour: $M_B < \mu_{AC}$ is met as Se is replaced with S. Linear behaviour is expected within the two-mode system, so the fitting shown in Figure 6b is valid, producing expressions ω_{CZTSe} (cm^{-1}) = $(44.6 \pm 1.6)x + (194.6 \pm 0.8)$ for the CZTSe-like A mode, and ω_{CZTS} (cm^{-1}) = $(7.1 \pm 1.3)x + (329.0 \pm 0.8)$ for the CZTS-like A mode. This offers consistency with values reported by Adachi (whose review combined the work of Grossberg *et al.*[9] and He *et al.*[10]) for CZTSe: ω_{CZTSe} (cm^{-1}) = $46.8x + 194.9$, but differs from the reported values for CZTS: ω_{CZTS} (cm^{-1}) = $12.2x + 324.5$[11]. Compared to literature values, we observe a less rapid variation with composition in the case of the CZTS modes, a large part of which may be attributed to a greater (extrapolated) wavenumber value at $x = 0$. As with the Vegard relationship, we may place additional confidence in our values for this trend given the large number of data points and the accurate determination of elemental composition. The samples employed by Grossberg *et al.* and He *et al.* were copper-poor, and since Lafond *et al.*, among others, have demonstrated the sensitivity of lattice parameters to cation composition[23], it is possible in principle that this will influence both the linear coefficient and $x = 0$ values for the CZTS-like mode.

CONCLUSIONS

Solid solutions over the full composition range of the $Cu_2ZnSnS_{4x}Se_{4-4x}$ (CZTSSe) series with intervals of $\Delta x = 0.1$ were synthesised from elements, with compositions near to stoichiometry. These were then crystallised from solution in molten NaCl/KCl giving compact deposits on the silica tube walls or on silica nucleation plates included in the growth tubes.

Powder XRD for the crystallised materials gave linear Vegard's relations a (Å) = $-0.268(3)x + 5.6949(17)$ and c (Å) = $-0.516(6)x + 11.345(3)$ for the lattice parameters, while the principal Raman modes varied as ω_{CZTSe} (cm^{-1}) = $(44.6 \pm 1.6)x + (194.6 \pm 0.8)$ for the CZTSe-like A mode, and ω_{CZTS} (cm^{-1}) = $(7.1 \pm 1.3)x + (329.0 \pm 0.8)$ for the CZTS-like mode. These data will be of use as fundamental reference data in the characterisation of thin-film CZTSSe, since they have been established with higher precision than in earlier reports. Compared to the results of x determination using lattice parameter from the data in our study, previous studies would give compositional discrepancies of up to ± 0.08 from a, and overestimates by as much as $+0.19$ from the use of c. While the exact reason

for the difference is not known, our results refer to slightly Cu-rich compositions, which may well play a key role. Our Raman data gave a reliable linear fit for the CZTSe-like modes, but more scatter was present in the variation of CZTS mode wavenumbers with composition, making the CZTSe modes more reliable for use in composition evaluation. Hence we recommend the variation of the lattice parameter a and the variation of the CZTSe-like Raman band as being the most reliable for composition determination.

The influence of crystallisation was to increase the ordering in the materials, which transformed from being disordered kesterite in the as-synthesised feedstock to being more ordered kesterite in the crystallised samples. This caused a shift in the principal peaks to higher energies.

SUPPORTING INFORMATION

Supporting information is available. Figures S1-S8 covering: DSC; SEM; metallographic analysis; determination of elemental proportions from weighing, EDX and ICP-OES; residual plots from Rietveld refinement; comparison of trends in lattice parameter with literature; FWHM change with x - value. Tables S1-S3 cover: complete elemental proportions determined by all methods; fitting parameters for Rietveld refinement and structural results. Text covers Rietveld refinement methodology.

REFERENCES

(1) Yan, C.; Huang, J.; Sun, K.; Johnston, S.; Zhang, Y.; Sun, H.; Pu, A.; He, M.; Liu, F.; Eder, K.; Yang, L.; Cairney, J. M.; Ekins-Daukes, N. J.; Hameiri, Z.; Stride, J. A.; Chen, S.; Green, M. A.; Hao, X. Cu_2ZnSnS_4 solar cells with over 10% power conversion efficiency enabled by heterojunction heat treatment. *Nat. Energy* **2018**, 3, 764-774.

(2) Taskesen, T.; Neerken, J.; Schoneberg, J.; Pareek, D.; Steininger, V.; Parisi, J.; Gütay, L. Device characteristics of an 11.4% CZTSe solar cell fabricated from sputtered precursors. *Adv. Energy Mater.* **2018**, 8, 1703295.

(3) Wang, W.; Winkler, M. T.; Gunawan, O.; Gokmen, T.; Todorov, T. K.; Zhu, Y.; Mitzi, D. B. Device characteristics of CZTSSe thin-film solar cells with 12.6% efficiency. *Adv. Energy Mater.* **2014**, 4, 1301465.

(4) Schorr, S. Crystallographic aspects of Cu_2ZnSnS_4 (CZTS). In *Copper Zinc Tin Sulfide-Based Thin-Film Solar Cells*; Ito, K., Ed.; John Wiley and Sons: Chichester, 2015; pp 55–74.

(5) Grossberg, M.; Krustok, J.; Raudoja, J.; Raadik, T. The role of structural properties on deep defect states in Cu_2ZnSnS_4 studied by photoluminescence spectroscopy. *Appl. Phys. Lett.* **2012**, 101, 102102.

(6) Lafond, A.; Ericson, T.; Scragg, J. S. A Low-temperature order-disorder transition in Cu_2ZnSnS_4 thin films. *Appl. Phys. Lett.* **2014** 104, 041911.

(7) Nagaoka, A.; Yoshino, K.; Taniguchi, H.; Taniyama, T. Growth and characterization of $Cu_2ZnSn(S_xSe_{1-x})_4$ alloys grown by the melting method. *J. Cryst. Growth* **2014**, 386, 204–207.

(8) Nagaoka, A.; Katsube, R.; Nakatsuka, S.; Yoshino, K. Growth and characterization of $Cu_2ZnSn(S_xSe_{1-x})_4$ single crystal grown by traveling heater method. *J. Cryst. Growth* **2015**, 423, 9–15.

(9) Grossberg, M.; Krustok, J.; Raudoja, J.; Timmo, K.; Altosaar, M.; Raadik, T. Photoluminescence and Raman study of $Cu_2ZnSn(Se_xS_{1-x})_4$ monograins for photovoltaic applications. *Thin Solid Films* **2011**, 519, 7403–7406.

(10) He, J.; Sun, L.; Chen, S.; Chen, Y.; Yang, P.; Chu, J. Composition dependence of structure and optical properties of $Cu_2ZnSn(S,Se)_4$ solid solutions: An experimental study. *J. Alloys Compd.* **2011**, 511, 129–132.

(11) Adachi, S. Mechanical and lattice dynamic properties In *Copper Zinc Tin Sulfide-Based Thin-Film Solar Cells*; Ito, K., Ed.; John Wiley and Sons: Chichester, 2015; pp 149–162.

(12) Ionkin, A. S.; Fish, B. M.; Marshall, W. J.; Senigo, R. H. Use of inorganic fluxes to control morphology and purity of crystalline késterite and related quaternary chalcogenides. *Sol. Energy Mater. Sol. Cells* **2012**, 104, 23–31.

(13) Mellikov, E.; Altosaar, M.; Kauk-Kuusik, M.; Timmo, K.; Meissner, D.; Grossberg, M.; Krustok, J.; Volobujeva, O. Growth of CZTS-based monograins and their application to membrane solar cells. In *Copper Zinc Tin Sulfide-Based Thin-Film Solar Cells*; Ito, K., Ed.; John Wiley and Sons: Chichester, 2015; pp 239–310.

(14) Raadik, T.; Krustok, J.; Kauk-kuusik, M.; Timmo, K.; Grossberg, M.; Ernits, K.; Bleuse, J. Low temperature time resolved photoluminescence in ordered and disordered Cu_2ZnSnS_4 single crystals *Phys. B Condens. Matter Mater. Phys.* **2016**, 508, 47–50.

(15) Rey, G.; Redinger, A.; Sendler, J.; Weiss, T. P.; Thevenin, M.; Guennou, M.; El Adib, B.; Siebentritt, S. The band gap of $Cu_2ZnSnSe_4$: Effect of order-disorder. *Appl. Phys. Lett.* **2014**, 105, 112106.

(16) Mai, D.; Park, H.; Choi, I. Growth of Cu_2ZnSnS_4 crystals by the directional freezing method with an induction heater. *J. Cryst. Growth* **2014**, 402, 104–108.

(17) Rodriguez-Carvajal, J.; Recent advances in magnetic structure determination by neutron powder diffraction. *Phys. B (Amsterdam, Neth.)* **1993**, 192, 55-69.

(18) Ritscher, A.; Just, J.; Dolotko, O.; Schorr, S.; Lerch, M. A mechanochemical route to single phase Cu_2ZnSnS_4 powder. *J. Alloys and Compd.* **2016,** 16, 30328-0.

(19) Choubrac, L.; Lafond, A.; Paris, M.; Guillot-Deudon, C.; Jobic, S. The stability domain of the selenide kesterite photovoltaic materials and NMR investigation of the Cu/Zn disorder in $Cu_2ZnSnSe_4$ (CZTSe). *Phys. Chem. Chem. Phys.* **2015**, 17, 15088-15092.

(20) Nozaki, H.; Fukano, T.; Ohta, S.; Seno, Y.; Katagiri, H.; Jimbo, K. Crystal structure determination of solar cell materials: Cu_2ZnSnS_4 thin films using X-ray anomalous dispersion. *J. Alloys Compd.* **2012**, 524, 22-25

(21) Vigil-Galán, O.; Courel, M.; Espindola-Rodriguez, M.; Izquierdo-Roca, V.; Saucedo, E.; Fairbrother, A. Toward a high Cu_2ZnSnS_4 solar cell efficiency processed by spray pyrolysis method. *J. Renewable Sustainable Energy* **2013,** 5, 053137

(22) Choubrac, L.; Paris, M.; Lafond, A.; Guillot-Deudon, C.; Rocquefelte, X.; Jobic, S. Multinuclear (^{67}Zn, ^{119}Sn and ^{65}Cu) NMR spectroscopy – an ideal technique to probe the cationic ordering in Cu_2ZnSnS_4 photovoltaic materials. *Phys. Chem. Chem. Phys.* **2013**, 15, 10722.

(23) Lafond, A.; Choubrac, L.; Guillot-Deudon, C.; Deniard, P.; Jobic, S. Crystal structures of photovoltaic chalcogenides, an intricate puzzle to solve: The cases of CIGSe and CZTS materials. *Z. Anorg. Allg. Chem.* **2012**, 638, 2571-2577.

(24) Mkawi, E. M.; Ibrahim, K.; Ali, M. K. M.; Farrukh, M. A.; Allam, N. K. Influence of precursor thin films stacking order on the properties of Cu_2ZnSnS_4 thin films fabricated by electrochemical deposition method. *Superlattices Microstruct.* **2014**, 76, 339–348.

(25) Guo, L.; Zhu, Y.; Gunawan, O.; Gokmen, T.; Deline, V. R.; Ahmed, S.; Romankiw, L. T.; Deligianni, H. Electrodeposited $Cu_2ZnSnSe_4$ thin film solar cell with 7% power conversion efficiency. *Prog. Photovoltaics* **2014**, 22, 58–68.

(26) Zeng, X.; Tai, K. F.; Zhang, T.; Ho, C. W. J.; Chen, X.; Huan, A.; Sum, T. C.; Wong, L. H. $Cu_2ZnSn(S,Se)_4$ kesterite solar cell with 5.1% efficiency using spray pyrolysis of aqueous precursor solution followed by selenization. *Sol. Energy Mater. Sol. Cells* **2014**, 124, 55–60.

(27) Khare, A.; Himmetoglu, B.; Johnson, M.; Norris, D. J.; Cococcioni, M.; Aydil, E. S. Calculation of the lattice dynamics and Raman spectra of copper zinc tin chalcogenides and comparison to experiments. *J. Appl. Phys.* **2012**, 111, 83707.

(28) Valakh, M. Y.; Kolomys, O. F.; Ponomaryov, S. S. Yukhymchuk, V. O.; Babichuk, I. S.; Izquierdo-Roca, V.; Saucedo, E.; Perez-Rodriguez, A.; Morante, J. R., Schorr, S.; Bodnar, I. V. Raman scattering and disorder effect in Cu_2ZnSnS_4. *Phys. Status Solidi RRL* **2013,** 7, 258-261.

(29) Chang, I. F.; Mitra, S. S. Application of a modified random-element-isodisplacement model to long-wave optic phonons of mixed crystals. *Phys. Rev.* **1968**, 172, 924–933.

For table of contents use only.

Vegard relation and Raman band reference data generated from bulk crystals of kesterite phase composition series $Cu_2ZnSnS_{4x}Se_{4-4x}$ (CZTSSe $0 \leq x \leq 1$)

Authors
Theodore D. C. Hobson[1‡*], Oliver S. Hutter[1,4‡], Nicole Fleck[1], Luke M. Daniels[2], Jonathan D. Major[1], Tat Ming Ng[3] and Ken Durose[1]

1. Stephenson Institute for Renewable Energy / Dept. Physics, University of Liverpool, Peach St, Liverpool, L69 7ZF, UK.
2. Department of Chemistry, University of Liverpool, Crown Street, Liverpool, L69 7ZD, UK.
3. Department of Chemistry/Centre for Sustainable Chemical Technologies, University of Bath, Bath BA2 7AY, UK. Now at: Department of Mathematics, Physics and Electrical Engineering,
4. Northumbria University at Newcastle, Ellison Place, Newcastle Upon Tyne, NE1 8ST, UK.
[*]Corresponding author.

Author Contributions
The manuscript was written with contributions from all authors. All authors have given approval to the final version of the manuscript. ‡These authors contributed equally.

TOC Graphic
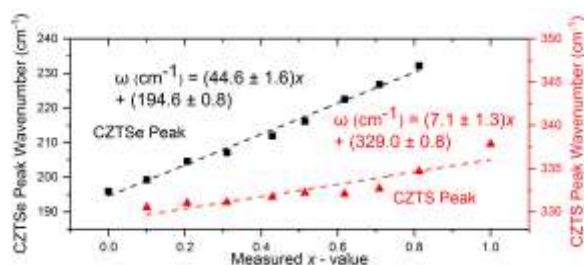
Synopsis

$Cu_2ZnSnS_{4x}Se_{4-4x}$ monograins crystallised from solution in a NaCl/KCl mix are studied with powder XRD and single-crystal Raman spectroscopy. Ordering effects are demonstrated and high-quality reference data is generated on the evolution of lattice parameter and Raman-active vibrational modes with S-Se ratio. Parameters are reported alongside accurately determined elemental proportions from ICP-OES measurements.